Investigation of Lens Aberrations through use of Phase Shifting Structures at 365nm Technology

James Guerrero
Microelectronic Engineering
Rochester Institute of Technology
Rochester, NY 14623

Abstract– As CMOS technology pushes feature dimensions beyond the sub-wavelength threshold, the effect of lens aberrations in the imaging system becomes more relevant. Therefore, it becomes important that the optical engineer completely understands the effects lens aberrations have on aerial image and resist profile. It is also important to have a tool and a process that can accurately describe and measure the aberrations in the exposure system. With full characterization of the lens systems and through use of a lithographic simulator, it becomes possible to predict the imaging effects and ultimately critical dimensions and pattern placement.

In any exposure system there exists a unique set of aberrations, which will have an effect on the aerial image. These aberrations can cause focus shifts dependant on pattern orientation, asymmetric imaging, degradation of image contrast, edge slope, pattern fidelity, resolution, and additional imaging artifacts. This paper looks at the use of a phase shifting ring structure of π radians phase shift and a lithographic simulator (PROLITH) for examination of lens aberrations in terms of Zernike coefficients Z_5 through Z_{11} (astigmatism – trifoil), Strehl ratio and wavefront OPD for a 365nm exposure system.

1. INTRODUCTION

When pushing the resolution limits of your optical systems, it becomes increasingly important to understand and predict its behavior. As feature dimensions go beyond the sub-wavelength threshold, the amount of system characterization that must be performed to adequately predict the system's behavior increases significantly. Part of the reason can be given to the relationship the effect of lens aberration have on an optical system; as feature dimensions decrease the effect of the lens aberration on the imaged pattern becomes more relevant.

Lens aberrations can be defined as the deviation of the real performance of an imaging system from the ideal. These deviations can be caused by many different reasons such as, variations in thickness, index of refraction, crystal orientation or defects in design [1]. When radiation passes through an ideal optical system, the resulting wavefront is perfectly spherical and can be predicted using Fourier optics; the resulting wavefront from a real optical system will deviate from this ideal wavefront and be a function of pupil position. The errors in phase or optical path difference (OPD) can therefore be quantified using a tool know as the Zernike polynomial. The Zernike polynomial is an infinitely long orthogonal polynomial, which is a mathematical attempt at reconstructing the post aberrated spherical wavefront. It is the polarity and magnitude of the coefficients of the Zernike polynomial that determines the amount of phase error that will be seen [2]. Each of the coefficients of the Zernike polynomial is a representation of a different type of aberration. Figure 1 shows the Zernike polynomial truncated at the 1st 36 terms.

Figure 1: First 36 terms of Zernike polynomial

```
z1 = 1;
z2 = ρ Cos[θ];
z3 = ρ Sin[θ];
z4 = -1 + 2 ρ^2;
z5 = ρ^2 Cos[2 θ];
z6 = ρ^2 Sin[2 θ];
z7 = ρ (-2 + 3 ρ^2) Cos[θ];
z8 = ρ (-2 + 3 ρ^2) Sin[θ];
z9 = 1 - 6 ρ^2 + 6 ρ^4;
z10 = ρ^3 Cos[3 θ];
z11 = ρ^3 Sin[3 θ];
z12 = ρ^2 (-3 + 4 ρ^2) Cos[2 θ];
z13 = ρ^2 (-3 + 4 ρ^2) Sin[2 θ];
z14 = ρ (3 - 12 ρ^2 + 10 ρ^4) Cos[θ];
z15 = ρ (3 - 12 ρ^2 + 10 ρ^4) Sin[θ];
z16 = -1 + 12 ρ^2 - 30 ρ^4 + 20 ρ^6;
z17 = ρ^4 Cos[4 θ];
z18 = ρ^4 Sin[4 θ];
z19 = ρ^3 (-4 + 5 ρ^2) Cos[3 θ];
z20 = ρ^3 (-4 + 5 ρ^2) Sin[3 θ];
z21 = ρ^2 (6 - 20 ρ^2 + 15 ρ^4) Cos[2 θ];
z22 = ρ^2 (6 - 20 ρ^2 + 15 ρ^4) Sin[2 θ];
z23 = ρ (-4 + 30 ρ^2 - 60 ρ^4 + 35 ρ^6) Cos[θ];
z24 = ρ (-4 + 30 ρ^2 - 60 ρ^4 + 35 ρ^6) Sin[θ];
z25 = 1 - 20 ρ^2 + 90 ρ^4 - 140 ρ^6 + 70 ρ^8;
z26 = ρ^5 Cos[5 θ];
z27 = ρ^5 Sin[5 θ];
z28 = ρ^4 (-5 + 6 ρ^2) Cos[4 θ];
z29 = ρ^4 (-5 + 6 ρ^2) Sin[4 θ];
z30 = ρ^3 (10 - 30 ρ^2 + 21 ρ^4) Cos[3 θ];
z31 = ρ^3 (10 - 30 ρ^2 + 21 ρ^4) Sin[3 θ];
z32 = ρ^2 (-10 + 60 ρ^2 - 105 ρ^4 + 56 ρ^6) Cos[2 θ];
z33 = ρ^2 (-10 + 60 ρ^2 - 105 ρ^4 + 56 ρ^6) Sin[2 θ];
z34 = ρ (5 - 60 ρ^2 + 210 ρ^4 - 280 ρ^6 + 126 ρ^8) Cos[θ];
z35 = ρ (5 - 60 ρ^2 + 210 ρ^4 - 280 ρ^6 + 126 ρ^8) Sin[θ];
z36 = -1 + 30 ρ^2 - 210 ρ^4 + 560 ρ^6 - 630 ρ^8 + 252 ρ^10;
```

The primary aberrations astigmatism, coma, spherical and trifoil are represented by Zernike coefficients Z_5 - Z_{11}. These primary aberrations are slightly easier to detect in an imagines system due to the characteristic effects they have on printed images [3]. For example, the astigmatism 0/90° and 45° directions, Z_5 and Z_6, can account for focus shifts dependant on image orientation leading to horizontal, vertical or 45° biases. The coma aberrations along the x and y directions, Z_7 and Z_8, are responsible for the

asymmetric printing of normally symmetric features. The Z_9 coefficient, spherical aberration, is a close relative of the defocus aberration and can cause degradation of image contrast, edge slope, pattern fidelity, and resolution. The trifoil aberrations, Z_{10} and Z_{11}, along the 0° and 30° directions can account for undesired imaging artifacts at three-fold asymmetry [2].

2. THEORY

Once a good understanding of the effects lens aberrations has on an imaging system is acquired and a tool exists for quantifying the aberrations, a method must be generated to effectively measure the aberrations in a system in an accurate and cost efficient manor. There are a few approaches that can be taken in light of aberration detection. The first and simplest method can be done using an ideal point source, and examining its Fourier transform, which is the $\text{sinc}^2()$ function about all azimuthal angles or the somb() function. So deviations in the resulting point spread function (PSF) can be directly related to certain aberrations and ultimately Zernike coefficients. The only problem with this approach is that as the source approaches the ideal point source case, the intensity approaches zero. Figures 2 and 3 show the coherent source and its respective point spread function with 0.5 waves of x coma, Z_7, added.

Figure 2: Coherent Illumination Source

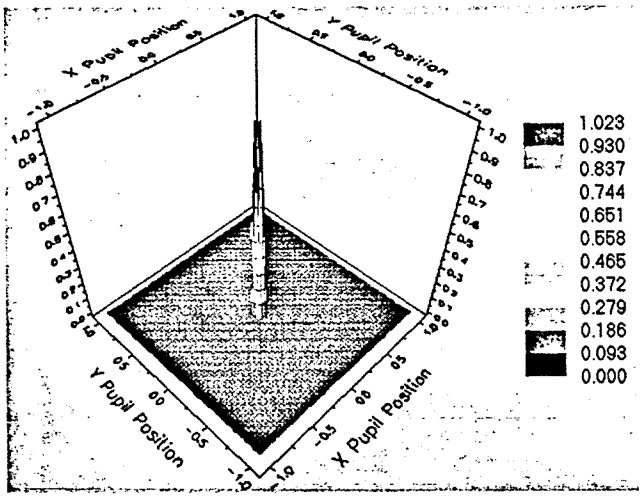

Figure 3: Point spread function with 0.5 waves of Z_7 coma

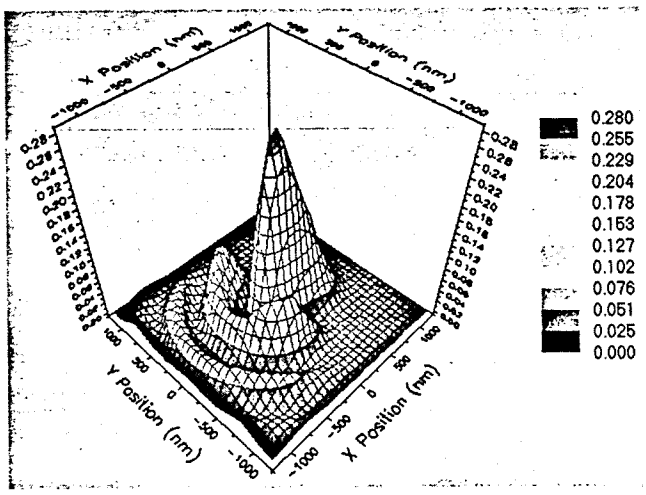

The line spread function is another way to detect lens aberrations and it can be created using a 0 to π radian phase shift. The phase shift will print a line that is the minimum printable resolution for a given optical system. Figure 4 shows the phase structure and figure 5 shows the resultant image intensity. It is possible to image the phase line and investigate the effect the aberrations have on the printed pattern. The difficulty in using this structure is the aberration analysis is limited to a single direction, so it would be impossible to detect aberrations such as trifoil with this structure.

Figure 4: $0 - \pi$ radian phase shift

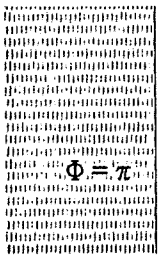

Figure 5: Phase shift relative intensity

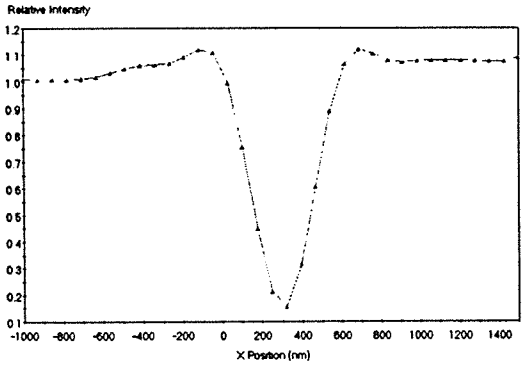

To solve both the intensity and directional problems, the line spread function can be copied along all azimuthal angles to produce a structure known as the Dirksen Aberration Ring shown in figure 6 [3]. The electric filed at the reticle, shown in figure 7, will change from positive to negative corresponding to the phase shift from 0 to π radians. The respective electric field at the wafer, shown in figure 8, follows the mask electric field with a slight sidewall slope added. The corresponding aerial image, shown in figure 9, would be proportional to the square of the amplitude function, therefore printing an annular ring as depicted by figure 10. The Dirksen ring allows investigation of each of several aberrations in any direction. The circular ring structure experiences a change in the shape of the inner and outer contour of the ring and a change in the distance between these contours, this allows for the detection of the aberrations independently of each other [3].

Figure 6: Dirksen aberration ring mask design

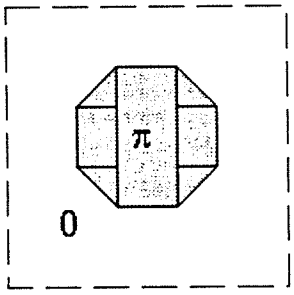

Figure 7: Mask electric field

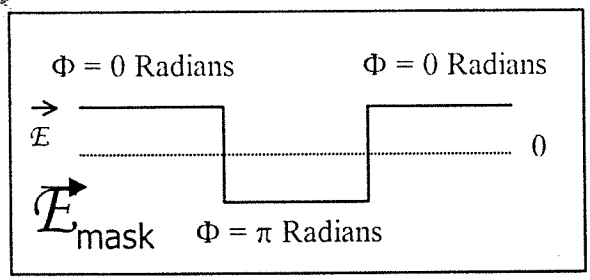

Figure 8: Wafer electric field

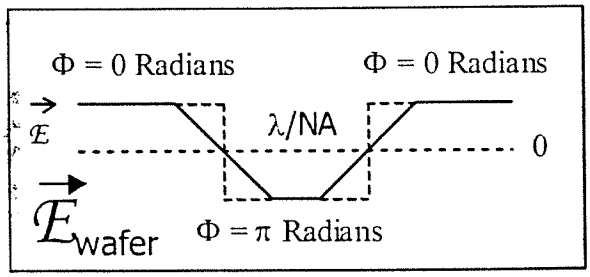

Figure 9: Aerial image

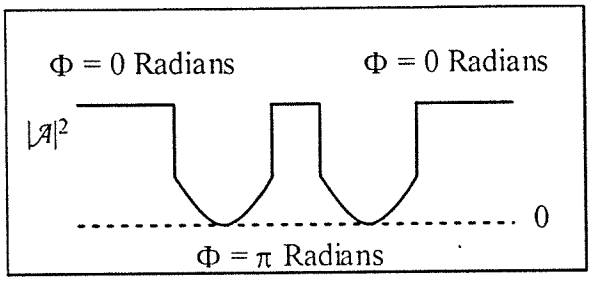

Figure 10: Printed aberration ring

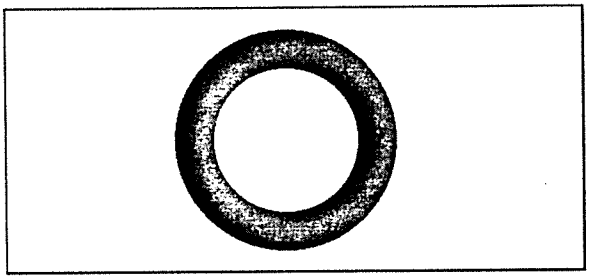

3. EXPERIMENT

A. Measurement Process

The aberration measurement process used, shown in figure 11, can be broken down into three main parts: SEM image collection, simulation and image correlation. First the aberration ring reticle was designed, fabricated and exposed on 200mm wafers through a focus of −1.5 to 0.1μm. The images were captured with a Hitachi CD SEM coupled with an image capture device. The experimental conditions and the phase ring structure were input PROLITH and simulated. The simulated aberration rings were then compared to the collected SEM images and values of Zernike coefficients were added and re-simulated until the simulated phase ring behavior through focus resembled that of the SEM collected phase ring. Preliminary simulation runs were performed to distinguish the behavior of the different aberrations though focus. Values of Zernike coefficients for each of the primary aberrations, $Z_5 - Z_{11}$, were added and varied as an input to PROLITH and the phase ring was simulated through focus.

Figure 11: Measurement process

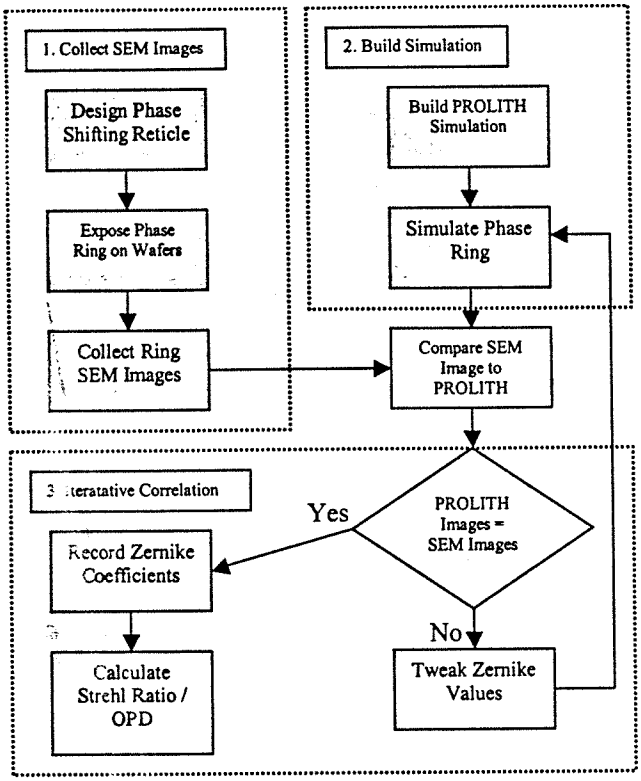

B. Phase Shift Mask Design

The phase shifting mask was designed on the CAD design tools as shown in figure 12. The diameter of the ring was designed according to the equation:

$$CD = \frac{\lambda}{NA} \qquad (1)$$

This was done to ensure that the line thickness of the phase ring was sub-resolution. If the phase ring line thickness is sub-resolution, the effects of the aberrations will be magnified enough for visual inspection.

The thickness of the quartz reticle had to be modified in the areas of the π radian phase shift. Deviations in the quartz thickness of the reticle would correspond to deviations in phase of the transmitted radiation. So a quartz etching process had to be designed to etch the desired thickness. The quartz step height was calculated using the following equation:

$$\Delta\Phi = \frac{2\pi}{\lambda}(n_{quartz} - 1)t \qquad (2)$$

Figure 12: Phase shifting mask cross-section and governing equations

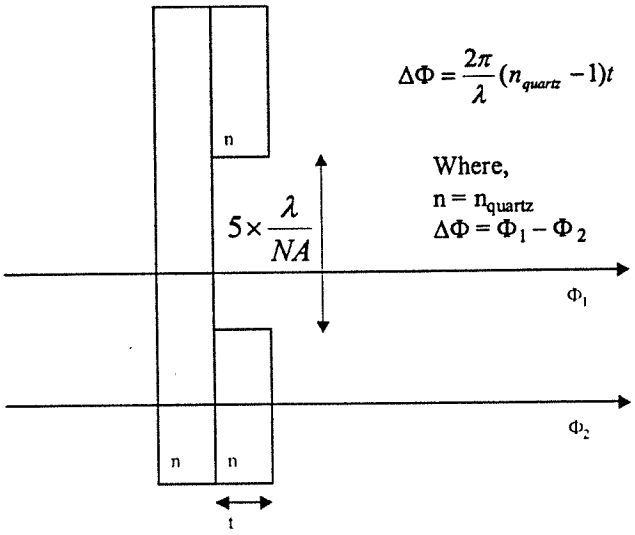

Using equation 1 the phase ring diameter was calculated to be 0.7μm. Making use of equation 2 and 1.47454, the index of refraction for fused silica, the step height of the phase shifting structure was calculated to be 384.5nm for a subsequent phase shift of π radians.

C. Experimental Conditions

Table 1: Experimental conditions

Parameter	Experimental	Simulated
Dose (mJ/cm2)	146	146
Coherence	0.6	0.6
Numerical Aperature	0.52	0.52
Resist Type	Olin620-10	Olin620-10
Resist Thickness (μm)	0.5	0.5
Ring Diameter (μm)	0.77	0.7
Quartz Step Height (nm)	410.2	410.2
Calculated Phase Shift (degrees)	192	192

4. RESULTS

The photoresist available, Olin OIR620-10, was optimized by the manufacturer to be coated at a thickness of 1μm; this was too thick for the experiment. In order to minimize the sidewall angles of the exposed phase ring and avoid false aberrations from being incorporated into the data, the resist had to be thinned to allow for about 0.5μm coating. The resist was thinned out with solvent, AZ photoresist thinner, and spin speed curves were

generated to allow for the targeted 0.5mm thickness. The final resist to solvent ratio was 5:1.

For the phase shifting reticle, a plasma etch process had to be created to give the desired thickness deviation in the fused silica to allow for a 0 to π radian phase shift. Preliminary etches were run to calculate the CHF_3 etch rate on fused silica. The test reticle was etched and the resultant step height was measured the profilometer to be 410.2mm which, using equation 2, resulted a phase shift of 192 degrees. The printed phase rings were measured on the CD SEM to be 0.77μm and were measured through a focus deviation of −1.5 to 0.7μm.

The simulations were performed using PROLITH. A full resist model was used to simulate the phase structures and the exposure conditions were modeled after the experimental conditions. Preliminary simulation runs were performed to investigate the behavior of the individual aberrations through a focus offset of −1.5 to 0.7μm. Figures 13 – 16 show some of the results of these preliminary simulations.

Figure 13: Astigmatism 0/90° (Z_5) through focus

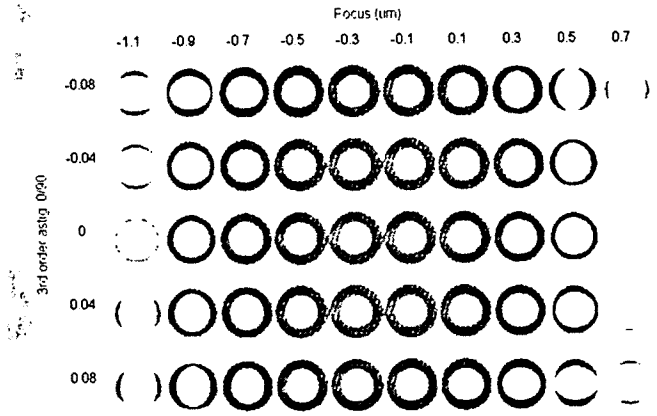

Figure 14: Astigmatism 45° (Z_6) through focus

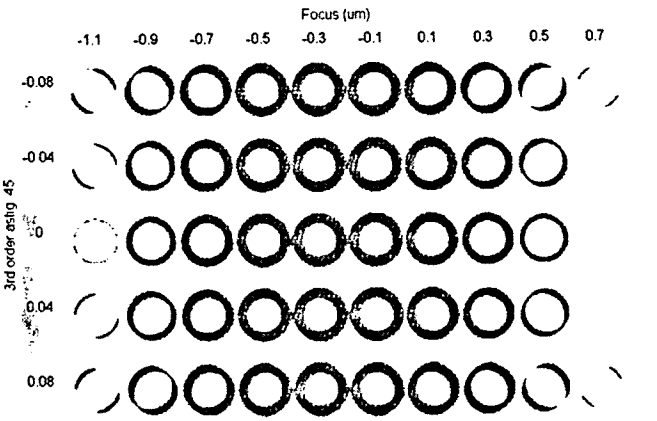

Figure 15: Coma X (Z_7) through focus

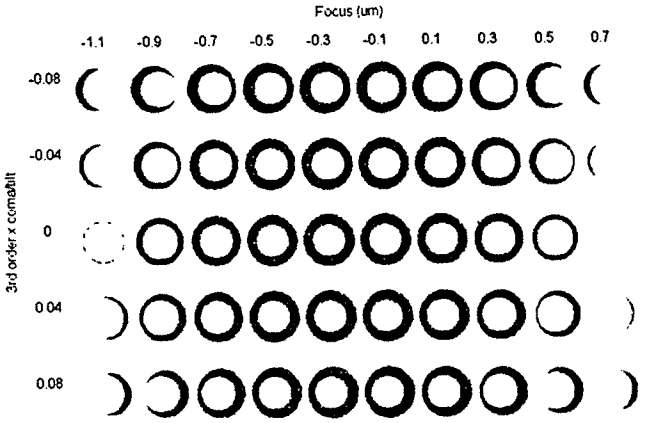

Figure 16: Coma Y (Z_8) through focus

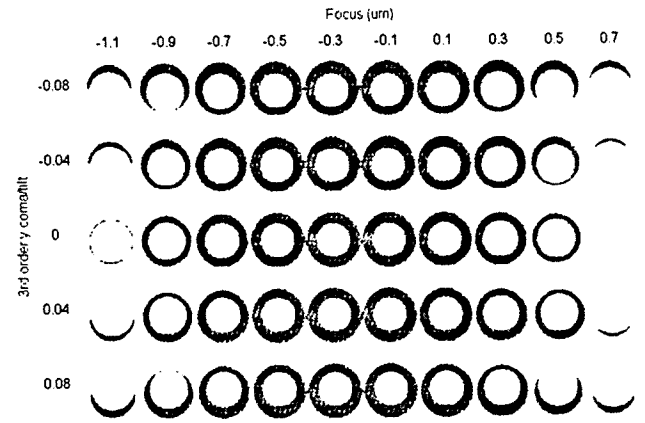

A vertical to horizontal shift in the primary axis through positive focus resulted in a negative coefficient for Z_5; conversely a horizontal to vertical primary axis shift corresponded to a positive coefficient for Z_5. Likewise a –45° to +45° primary axis shift through positive focus resulted in a negative coefficient of Z_6, conversely a primary axis shift of and a +45° to -45° gave rise to a positive coefficient for Z_6. The shifting of the position of the inner centroid was determined by the amount of coma in the system. A right shift in centroid position through positive focus resulted in a negative coefficient for Z_7. A downward shift in centroid position through positive focus resulted in a negative coefficient for coma Z_8. Spherical aberration, Z_9, resulted in a degradation of the phase ring contrast and a sloped resist sidewall. Trifoil, Z_{10} and Z_{11}, resulted in additional artifacts at three-fold asymmetry.

The SEM images were then visually inspected and the behavior through focus was examined. Figures 17 and 18 show a phase ring captured on the CD SEM through focus and aberration trends are graphically displayed. It can be seen that though positive focus there was a vertical to

horizontal primary axis shift, which showed the presence of a negative value for 0/90° astigmatism. Also through positive focus it was shown that –45° to +45° shift in primary axis, which showed a negative coefficient for 45° astigmatism. There was also a downward and to the right shift in the inner centroid position which corresponded to negative vales for x and y direction coma.

Figure 17: Phase ring SEM image –0.7 μm focus offset

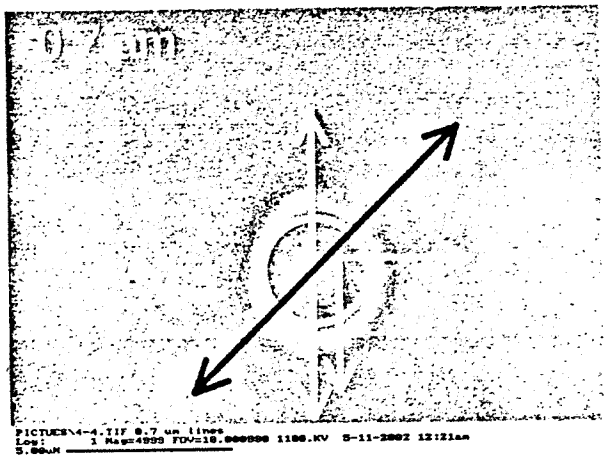

Figure 18: Phase ring SEM image –0.5 μm focus offset

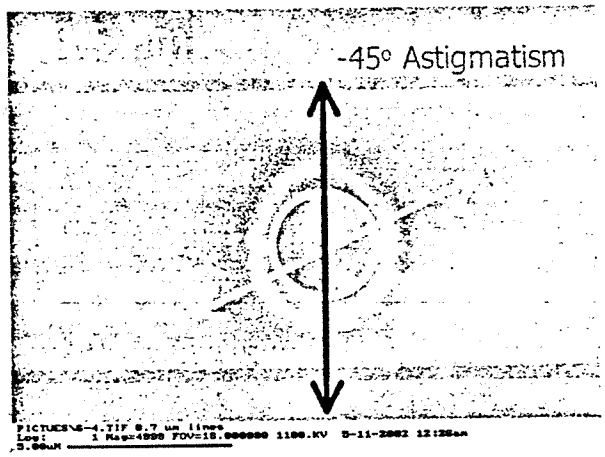

5. SUMMARY

The 365nm projection stepper system was measured to have a significant amount of astigmatism 0/90°, astigmatism 45° and spherical aberrations. The coma terms were present in both x and y directions, but were not as prominent as the astigmatism terms; this was also the case for the trifoil terms. Table 2 summaries the dominant aberrations in the optical system.

Table 2: Observed dominant aberrations

Dominant Aberration Terms	Zernike Coefficient
-0/90 Astigmatism	Z5
-45 Astigmatism	Z6
+Spherical	Z9

There were a few difficulties in obtaining high quality SEM images, which made it difficult to calculate accurate numbers for Zernike coefficients. This may have been due to the fact that the phase rings were patterned in photoresist, which may have led to charging issues when using the SEM. A very thin conductive layer could have been used which might have resolved the charging issue. Also, ideally the aberration investigation should be done as close to a perfect point source as possible, coherent illumination, but the imaging system under investigation had a fixed partial coherence of 0.6, which may have led to the averaging of the aberrations making it more difficult to determine the single effects. There were also difficulty in obtaining a tight control over the etch rate in the plasma etcher, which resulted in the over etching of the quartz reticle, this incorporated a slopes resist profile on the inner centroid. Addressing these issues would result in a more accurate estimation of the Zernike coefficients and calculation of wavefront OPD and Strehl ratio.

REFERENCES

[1] C. A. Mack, "Inside PROLITH: A Comprehensive Guide to Optical Lithography Simulation", Finle Technologies, Inc., TX, p. 21-25, 1997.

[2] T. A. Brunner, "Impact of Lens Aberrations on Optical Lithography" IBM Journal of Research and Development, Optical Lithography Volume 41, Numbers 1/2, 1997.

[3] P. Dirksen and C. A. H. Juffermans, U.S. Patent No. 6,248,486 B1, Washington, DC: U.S. Patent and Trademark Office, 2001.

ACKNOWLEDGMENTS

The author acknowledges Dr. Bruce Smith's guidance in this work and Bruce Tolleson and Charles Gruener for equipment support.

James Guerrero, originally from Brooklyn, New York, received B.S in Microelectronic Engineering from Rochester Institute of Technology in 2002. He attained co-op work experience at Motorola SPS and Infineon Technologies Richmond with particular interests in optical lithographic simulation, characterization and metrology techniques.